JMEPEG (2005) 14:441-447
DOI: 10.1361/105994905X56205

1059-9495/$19.00

Multi-Phase Nanocrystalline Al Alloy with Superior Strength and Modulus at Elevated Temperatures

H. Luo, L.C. Zhang, and L. Shaw

(Submitted April 27, 2005; in revised form May 16, 2005)

A multiphase nanocrystalline $Al_{93}Fe_3Cr_2Ti_2$ alloy containing 30 vol% intermetallic particles was prepared via mechanical alloying, followed by hot extrusion. Systematic compressive tests and modulus measurements were performed as a function of temperature and strain rate. High strengths and moduli at both ambient and elevated temperatures were demonstrated. The results clearly indicated that the multiphase nanocrystalline $Al_{93}Fe_3Cr_2Ti_2$ alloy has great potential for structural applications. Furthermore, the strength of the multiphase nanocrystalline Al alloy at both room and elevated temperatures increased with the decrease in the grain size, suggesting that diffusional creep is suppressed in this alloy, even though the grain size of the alloy is below 100 nm.

Keywords aluminum alloy, elevated temperature, nanostructured materials, strength

1. Introduction

It is well known that nanocrystalline (nc) metals (with grain sizes <100 nm) possess superior mechanical properties such as high strength, high hardness, excellent wear resistance and superplasticity, exceeding those of coarse-grained counterparts (Ref 1-8). The microstructure, mechanical properties, and deformation mechanisms of nc metals have been the subject of intensive study in recent years (Ref 9-17). However, most of these studies focus on the behavior and properties of single-phase nc materials. In contrast, investigation on multiphase nc alloys at both ambient and elevated temperatures is scarce.

In an attempt to explore the potential high-temperature structural applications, Inoue et al. (Ref 1, 18) chose the $Al_{93}Fe_3Cr_2Ti_2$ alloy as a multiphase nc material for investigation because Fe, Cr, and Ti all have very low diffusivity and equilibrium solubility in face-centered-cubic (fcc)-Al (0.03 at.% Fe, <0.01at.%Cr, and <0.2at.%Ti). Low diffusivity and solubility are the basic requirements for preventing Ostwald ripening (Ref 19, 20). Thus, the $Al_{93}Fe_3Cr_2Ti_2$ alloy is expected to have good microstructural stability at elevated temperatures and therefore superior high-temperature strengths (Ref 4, 21-23). The $Al_{93}Fe_3Cr_2Ti_2$ alloy prepared by Inoue et al. (Ref 1, 21), is obtained via the gas atomization approach, followed by hot extrusion.

In this study, mechanical alloying (MA) followed by extrusion is used to prepare the multiphase nc alloy. The potential advantage using MA to prepare the nc $Al_{93}Fe_3Cr_2Ti_2$ alloys over the gas atomization approach is the possibility of making nc Al matrix composites with nano-reinforcements (i.e., nano/nano-Al composites) through blending the elemental constituents of the metallic matrix or prealloyed metallic powder with insoluble nano-reinforcements such as nano-SiC particles. Nano/nano-Al composites are expected to have better microstructural stability and thus higher elevated temperature strengths than those exhibited by the corresponding nc Al alloys. The expected high elevated-temperature strengths of the MA-processed $Al_{93}Fe_3Cr_2Ti_2$ alloy have indeed been demonstrated (Ref 24). The current study takes one step further to investigate the effect of grain sizes on the elevated-temperature strength and elastic modulus.

A fully dense nc $Al_{93}Fe_3Cr_2Ti_2$ alloy with an average grain size of 30-100 nm was prepared in this study. Uniaxial compressive tests were performed at different temperatures and stain rates. The reason for choosing the compressive test is that it has a relatively stable testing condition for obtaining a substantial amount of plastic strain, not strongly influenced by extraneous factors such as surface or internal defects, as well as not subjected to the necking instability (Ref 25, 26). Under tensile loading conditions, many nc materials have very limited ductility and cannot sustain a uniform tensile deformation for more than a few percent (Ref 27). The elastic modulus of the nc alloy is also determined as a function of temperature. High strengths and moduli are obtained at both ambient and elevated temperatures. These superior properties are discussed using the existing creep theories and the rule of mixtures to develop insights into the deformation mechanisms of this extruded nc $Al_{93}Fe_3Cr_2Ti_2$ alloy.

2. Experimental Procedure

Crystalline elemental powders were used to prepare an Al alloy with a nominal composition of $Al_{93}Fe_3Cr_2Ti_2$. The aluminum powder used had a purity of 99.5% with a mean particle size of 70 μm, whereas the corresponding values for iron, chromium and titanium powders used were 99.0, 98.5, and 99.5% as well as 50, 30, and 30 μm, respectively. MA was performed under an argon atmosphere using a modified Szeg-

This paper was presented at the International Symposium on Manufacturing, Properties, and Application of Nanocrystalline Materials sponsored by the ASM International Nanotechnology Task Force and TMS Powder Materials Committee, October 18-20, 2004, Columbus, OH.

H. Luo, L.C. Zhang, and **L. Shaw,** Department of Materials Science and Engineering, Institute of Materials Science, University of Connecticut, Storrs, CT. Contact e-mail: leon.shaw@uconn.edu.

vari attritor, which has been shown to be effective in preventing the formation of the dead zone and producing uniform milling products within the powder charge (Ref 28). The canister of the attritor was made of a stainless steel and the charge consisted of stainless balls with a diameter of 4.76 mm. A ball-to-powder weight ratio of 20:1 and a milling speed of 600 RPM with the milling duration of 30 h were used in the MA process. During milling the canister was cooled by circulation water with a flow rate of about 770 ml/min throughout the process. To prevent excessive cold welding of the Al alloy, 1.2 wt.% stearic acid [$CH_3(CH_2)_{16}COOH$] was added to the powder mixture as the process control agent at the beginning of the MA process (Ref 29).

Hot extrusion was used to convert the MA-processed powder to bulk material. Prior to extrusion, the MA-processed powder was containerized within a metal can and subjected to degassing which was carried out at a temperature ranging from 300-550 °C until the pressure of the can was reduced to 10^{-5} torr. The parameters controlled during extrusion included the angle of the extrusion dies, extrusion temperature, extrusion ratio, and strain rate. Based on a previous study (Ref 24), good extrusion conditions were used to prepare nc alloys with two different average grain sizes (one being 50 nm and the other 80 nm). Furthermore, to achieve a substantial amount of ductility under compressive loading, the continuous oxide film at the prior powder particle boundaries (PPB) was completely broken down under the extrusion conditions used (Ref 24).

The extruded $Al_{93}Fe_3Cr_2Ti_2$ bulk material was used to prepare cylindrical compressive specimens 6 mm in diameter and 9 mm in height. Both ends of the compressive specimens were polished to mirror surfaces and coated with MoS_2 before tests to reduce the interfacial friction. All the compressive tests were displacement controlled with a constant strain rate of 10^{-2}, 10^{-3}, or 10^{-4} s^{-1}. The tests were terminated if the specimen did not fracture at −0.45 true strain. The test temperature investigated ranged from 25 to 400 °C. The change of elastic modulus of the nc alloy with temperature was measured on a dynamic mechanical analyzer (DMA, 2980 from TA Instruments, Inc., New Castle, DE) in an argon environment with a heating rate of 3 °C/min.

The density of the extruded $Al_{93}Fe_3Cr_2Ti_2$ alloy was measured on the basis of Archimedes's principle. Furthermore, the extruded alloy was analyzed using x-ray diffraction (XRD, Bruker D8, BRUKER AXS, Inc., Madison, WI) with CuK_α radiation to monitor phase transformations and to estimate the crystallite size and internal strains of the fcc-Al phase in the nc $Al_{93}Fe_3Cr_2Ti_2$ alloy. The detailed procedure for estimating the crystallite size and internal strain can be found elsewhere (Ref 30, 31) and will not be repeated here.

Analyses of the grain size, crystal structure, and chemical composition within the microstructure of the Al alloy were also performed using a transmission electron microscope (TEM; Philips EM420) operating at 100 kV. In the TEM analysis, both bright- and dark-field image techniques coupled with selected area diffraction (SAD), convergent beam electron diffraction (CBED), and energy dispersive spectrometry (EDS) with an electron beam of 3.5 nm were used. TEM thin film samples were prepared by standard polishing steps and jet electropolishing at −30 °C after manually thinning the cut specimens to 100-μm-thick disks using a series of SiC abrasive papers. The electrolyte used in the jet electro-polishing consisted of 4% perchloric acid and 96% methanol. Chemical analyses of the extruded alloy were also performed using inductively coupled plasma-optical emission spectroscopy (ICP) in triplicate.

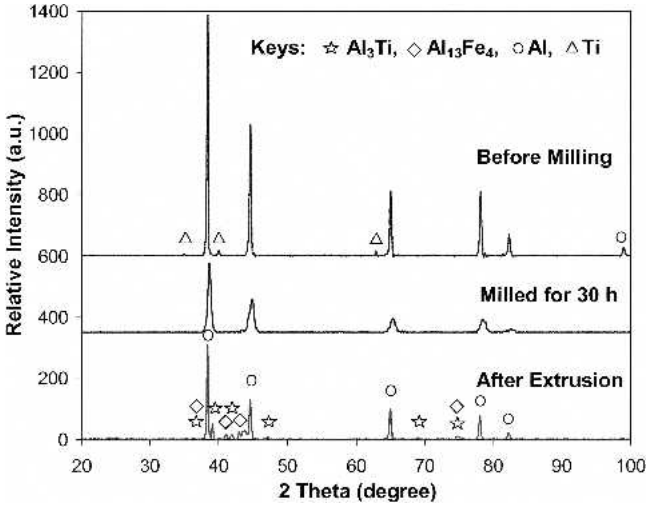

Fig. 1 XRD patterns of the $Al_{93}Fe_3Cr_2Ti_2$ alloy before ball milling, after ball milling for 30 h, and after hot extrusion at 500 °C. Note that after ball milling the alloy contains only the fcc-Al solid solution with substantial peak broadening, suggesting nanoscale fcc-Al grains. After extrusion at 500 °C, two additional phases, $Al_{13}Fe_4$ and Al_3Ti, are detected.

3. Results and Discussion

Figure 1 shows the XRD patterns of elemental powder mixtures with a nominal composition of the $Al_{93}Fe_3Cr_2Ti_2$ alloy before ball milling and after ball milling for 30 h and the extruded bulk alloy. The peak shifting to higher 2θ angles and peak broadening of Al reflections were noted after 30 h of ball milling. The peak shifting suggests the formation of an Al-based solid solution, whereas the peak broadening indicates the grain size refinement and/or the introduction of internal strains. The average grain size of the fcc-Al solid solution after 30 h milling, estimated using the Scherrer formula, is 14 nm, whereas the effective internal strain 2ξ, estimated using the Stokes and Wilson formula, is 1.8%. For the alloy extruded at 450 °C, three phases were identified from the XRD pattern and they are the fcc-Al solid solution, Al_6Fe, and Al_3Ti intermetallics. Similarly, the alloy extruded at 500 °C also contains three phases, but the metastable Al_6Fe phase has been replaced by the equilibrium phase, $Al_{13}Fe_4$.

Based on Archimedes's principle, the density of the alloy extruded at 450 °C was measured to be 2.92 g/cm^3, which is almost identical to 2.91 g/cm^3 calculated from the rule of mixtures with the assumptions that all Fe and Ti were present in the intermetallics, and thus the alloy was composed of 70% fcc-Al, 18% Al_6Fe, and 12% Al_3Ti (in volume percent). This result indicates the attainment of the full density of the extruded alloy and is in good agreement with the TEM examination and the SEM observation, which show no porosity in the alloy before etching.

The chemical compositions of the $Al_{93}Fe_3Cr_2Ti_2$ alloy before and after mechanical alloying analyzed using the ICP method are listed in Table 1. Because the addition of 1.2 wt.% stearic acid brings 0.91% carbon and 0.135% oxygen to the Al alloy, the chemical analysis indicates that the milling process

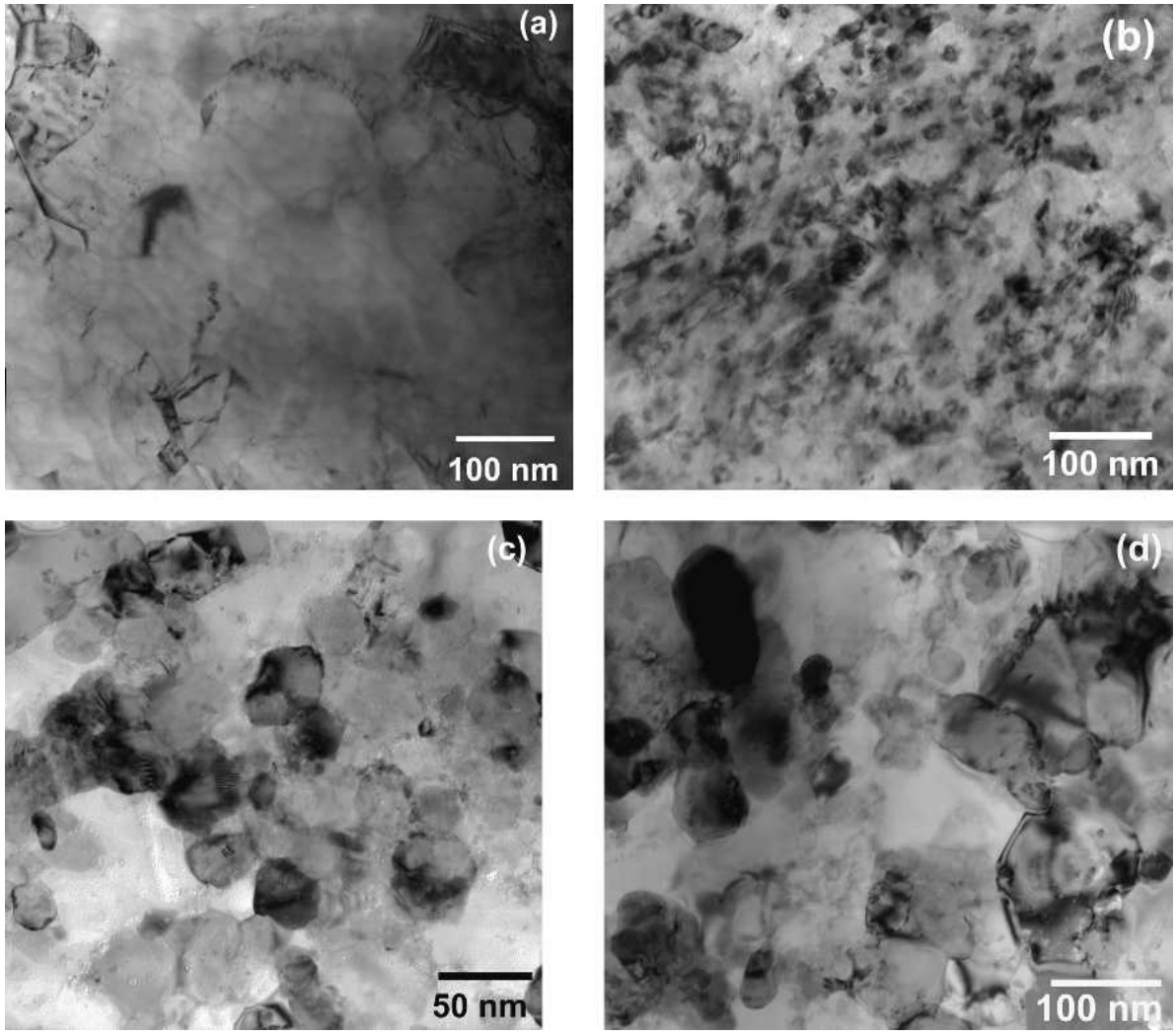

Fig. 2 TEM micrographs of the $Al_{93}Fe_3Cr_2Ti_2$ alloy: elemental Al powder (a) before ball milling, (b) after 30 h of ball milling, (c) after extrusion at 450 °C, showing an average grain size of 50 nm, and (d) after extrusion at 500 °C, showing an average grain size of 80 nm

Table 1 Chemical compositions of Al-Fe-Cr-Ti alloys under various conditions determined using ICP

Sample condition	Fe, wt.%	Cr, wt.%	Ti, wt.%	C, wt.%	O, wt.%	N, wt.%	Al, wt.%
Before milling without S.A.	5.82	3.61	3.33	0.026	0.462	0.0009	Bal
After milling with 1.2 wt.% S.A.	6.06	3.19	3.17	0.906	0.782	0.0175	Bal
After extrusion	5.99	3.41	3.19	1.076	1.267	0.0445	Bal

Note: S.A., stearic acid

does not introduce any additional carbon but does introduce 0.185% oxygen into the material. This result is obtained by subtracting the oxygen content present in the powder mixture before milling without stearic acid and that brought in by the addition of stearic acid from the total oxygen content after milling with 1.2 wt.% stearic acid. The Al alloy appears to pick up a small amount of oxygen and nitrogen in the extrusion process; however, the concentrations of all the other elements stay the same as before the extrusion process. If all the carbon and oxygen in the extruded alloy react with Al to form Al_4C_3 and Al_2O_3, the extruded Al alloy would contain 3.73 vol.% Al_4C_3 and 1.42 vol.% Al_2O_3. Because SAD patterns indicate no Al_4C_3 and Al_2O_3 phases, Al_4C_3 and Al_2O_3 are likely to be present in a noncrystalline form.

Shown in Fig. 2 are typical TEM bright-field images of the alloy before ball milling, after ball milling, and after the subsequent extrusion. Note that the starting Al powder before ball milling is composed of micrometer-size particles with micrometer grain sizes (Fig. 2a). After ball milling for 30 h, the fcc-Al grain size is reduced to 6-45 nm (Fig. 2b), basically substantiating the finding of the grain size of 14 nm estimated from the XRD analysis. The typical microstructures of the $Al_{93}Fe_3Cr_2Ti_2$ alloy extruded at 450 and 500 °C are shown in Fig. 2(c) and (d), respectively. Extrusion at 450 °C results in an average grain size of 50 nm for the fcc-Al, whereas extrusion at 500 °C leads to an average grain size of 80 nm. As noted previously, extruded $Al_{93}Fe_3Cr_2Ti_2$ alloys at both temperatures consist of intermetallic particles. Figure 3 shows the typical

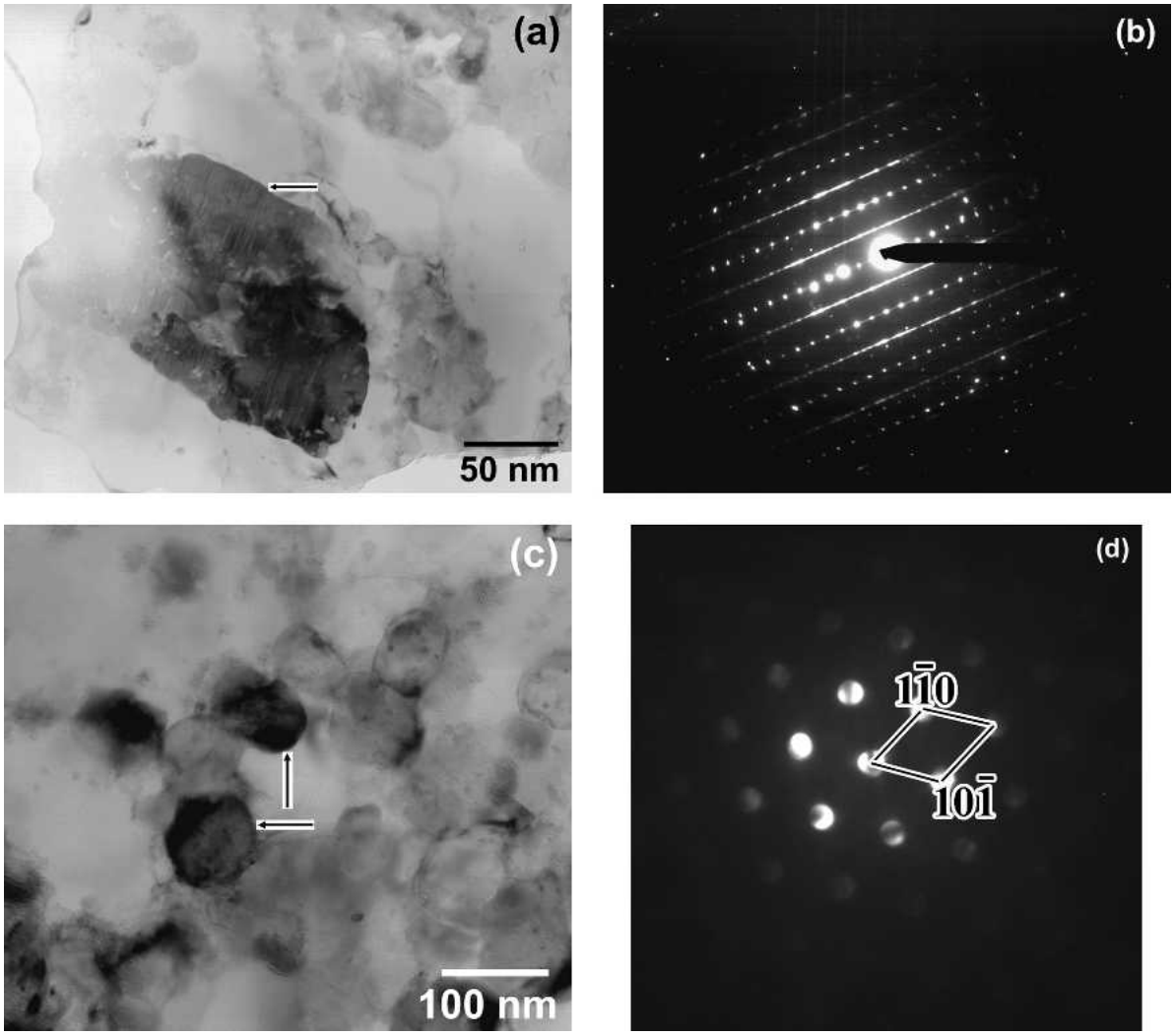

Fig. 3 TEM bright-field images of (a) $Al_{13}Fe_4$ and (c) Al_3Ti precipitates in the $Al_{93}Fe_3Cr_2Ti_2$ alloy extruded at 500 °C. The corresponding CBED patterns of $Al_{13}Fe_4$ and Al_3Ti precipitates are shown in (b) and (d), respectively.

morphologies of $Al_{13}Fe_4$ and Al_3Ti particles in the fcc-Al matrix and their corresponding CBED patterns. These intermetallic particles are precipitated during the extrusion process, and their sizes are similar to that of the fcc-Al grains.

Figure 4 shows the EDS results of the fcc-Al grains before and after extrusion. It can be seen that the fcc-Al grains before extrusion is a supersaturated solid solution with Fe, Cr, and Ti solutes. After extrusion the solute concentration in the fcc-Al grain becomes very low. In fact, it is below the EDS detection limit. The reduction of the solute concentration is consistent with the formation of intermetallic precipitates revealed in the XRD and TEM studies (Fig. 1, 2, and 3). The precipitation during extrusion has changed the supersaturated fcc-Al solid solution to the fcc-Al with very low solute concentrations. If the equilibrium solubility is reached during extrusion, the concentrations of Fe, Cr, and Ti in the fcc-Al grain would become 0.03 at.%, <0.01 at.%, and <0.2 at.%, respectively (Ref 19).

Typical true stress-true strain curves of the extruded nc $Al_{93}Fe_3Cr_2Ti_2$ alloys obtained from compressive tests with a strain rate of 10^{-3} s^{-1} at different temperatures are shown in Fig. 5. All specimens exhibit excellent compressive ductility in the tests at both ambient and elevated temperatures and therefore have great potential for structural applications. No cracks form at the interior or at the surface even after a true strain of −0.45, at which the compressive tests are terminated. Three samples are tested for each condition, and good repeatability is noted from these tests.

The strength of the extruded $Al_{93}Fe_3Cr_2Ti_2$ alloys is temperature and grain size dependent. The ultimate strength for the $Al_{93}Fe_3Cr_2Ti_2$ alloy with an average grain size of 80 nm (Fig. 5a) is about 670 MPa at room temperature, whereas the corresponding values are 445, 320, and 180 MPa at 200, 300, and 400 °C, respectively. In contrast, the ultimate strength for the $Al_{93}Fe_3Cr_2Ti_2$ alloy with an average grain size of 50 nm (Fig. 5b) is about 690 MPa at room temperature; the corresponding values are 530 and 340 MPa at 200 and 300 °C, respectively. These maximum strengths, especially those at elevated temperatures, compare very favorably against current commercially available and other reported tentative Al alloys, including Al-Ti-Cu (Ref 32), Al-Fe-Ce (Ref 33), Al-Fe-V-Si (Ref 34), and dispersion strengthened Al (Ref 35). All of the commercially available alloys lose their useful strengths when the temperature is above 250 °C (typically becoming lower than 200 MPa) (Ref 36). The superior high-temperature strength of the nc $Al_{93}Fe_3Cr_2Ti_2$ alloys is likely derived from the low diffusivities of the alloying elements, the presence of the na-

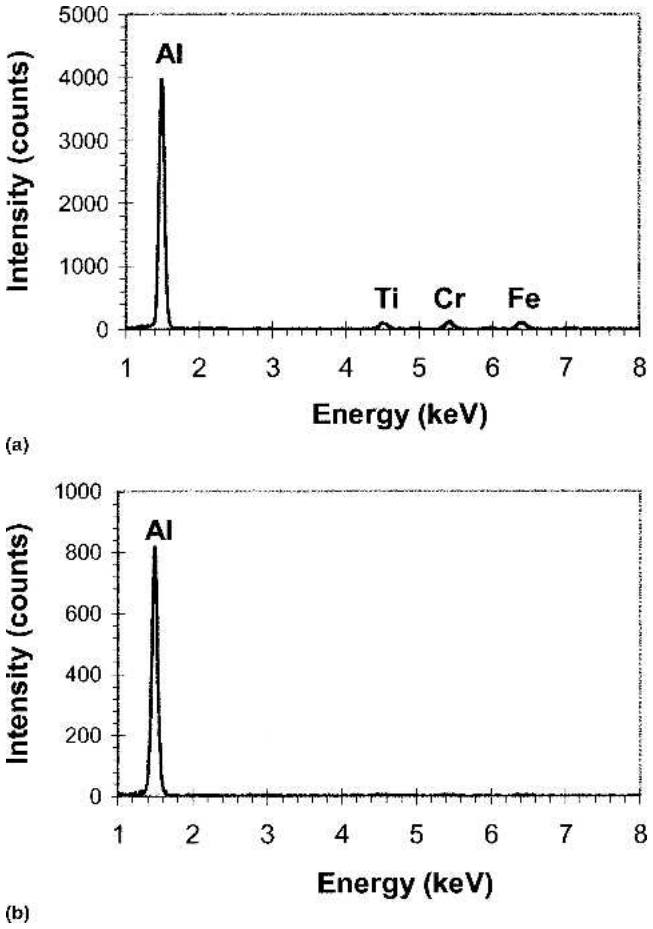

Fig. 4 EDS spectra of (a) the $Al_{93}Fe_3Cr_2Ti_2$ alloy before extrusion and (b) a fcc-Al grain in the nc alloy extruded at 450 °C

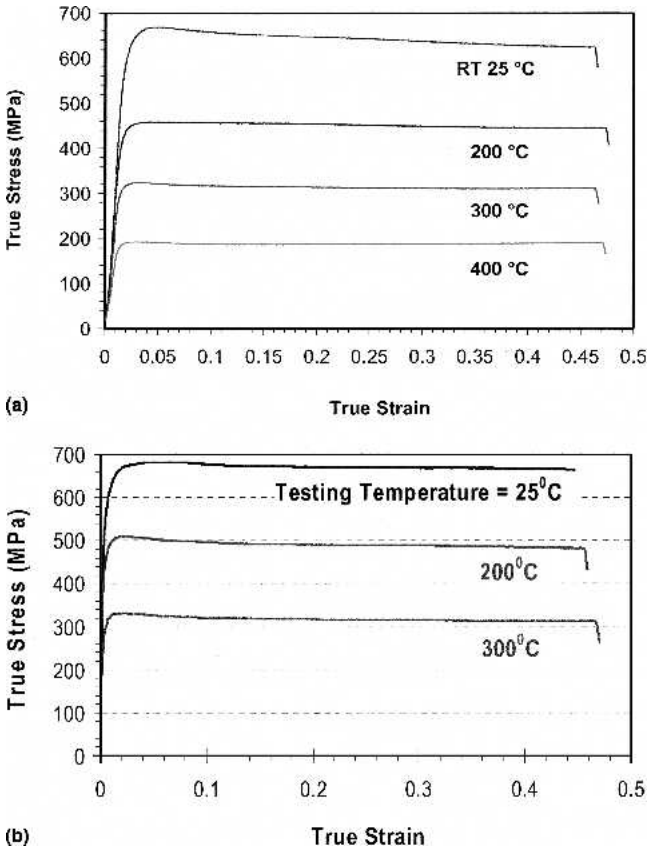

Fig. 5 Compressive true stress-true strain curves of the extruded nc $Al_{93}Fe_3Cr_2Ti_2$ alloy under a constant strain rate of 10^{-3} s^{-1} at different temperatures as indicated: (a) alloy extruded at 500 °C with an average grain size of 80 nm and (b) alloy extruded at 450 °C with an average grain size of 50 nm

noscale intermetallic precipitates, the retention of the nc Al grains after extrusion, and solid solution strengthening. However, the specific strengthening mechanisms are unclear at this stage and will be investigated in the near future.

Note that the result from the compressive test has clearly revealed a very interesting phenomenon: the strength of the multiphase nanocrystalline Al alloy increases with the decrease in the grain size at both ambient and elevated temperatures. This phenomenon strongly suggests that diffusional creep has been suppressed in these nc Al-alloys even at the homologous temperature of $0.78T_m$ (where T_m is the melting temperature of aluminum). It is well known that Coble creep can easily occur at this homologous temperature; furthermore, the finer the grain size, the lower the flow stress (Ref 37). The nc $Al_{93}Fe_3Cr_2Ti_2$ alloy in this study is clear in defying this general trend established from micrometer-grained materials. In fact, using the Coble creep formula (Ref 37):

$$\sigma = \dot{\varepsilon}_{Al} \frac{kT}{148\Omega} \frac{\pi d^3}{\delta D_{gb}} \quad \text{(Eq 1)}$$

an estimation of the flow stress for diffusional creep of the nc $Al_{93}Fe_3Cr_2Ti_2$ alloy can be made. σ in Eq 1 is the normal stress, $\dot{\varepsilon}_{Al}$ is the normal strain rate of the fcc-Al matrix, d is the average size of the fcc-Al grains, Ω is the atomic volume of aluminum, δ is the effective thickness of the grain boundary, D_{gb} is the diffusion coefficient at grain boundaries, and k and T have their usual meanings. Shown in Fig. 6 is the flow stress as a function of deformation temperature predicted from Eq 1 with the assumptions that (a) the average grain size of the fcc-Al grains is 50 nm, (b) all the diffusional parameters in Eq 1 are approximately equal to those provided by Frost and Ashby for pure Al (Ref 38), (c) the 30 vol.% intermetallic particles are not deformable, and (d) the effect of the nondeformable intermetallics is accounted for by the rule of mixtures (Eq 2):

$$\dot{\varepsilon}_C = \dot{\varepsilon}_{Al} \times 0.7 + \dot{\varepsilon}_{Int} \times 0.3 \quad \text{(Eq 2)}$$

where $\dot{\varepsilon}_C$ is the imposed strain rate in the compression test, and $\dot{\varepsilon}_{Int}$ is the strain rate of the intermetallics, which is zero due to the nondeformable assumption. Thus, the strain rate of the fcc-Al matrix in Eq. 1 is given by $\dot{\varepsilon}_{Al} = \dot{\varepsilon}_C/0.7$.

Figure 6 clearly reveals that the flow stress at high temperatures (i.e., $T > 100$ °C) for an imposed strain rate of 10^{-3} s^{-1} should be very low if Coble creep is operational in the nc $Al_{93}Fe_3Cr_2Ti_2$ alloy. For example, the predicted flow stress of 0.000158 MPa at 400 °C is 6 orders of magnitudes lower than the measured counterpart. Thus, there is no doubt that grain boundary diffusional creep is suppressed in the nc $Al_{93}Fe_3Cr_2Ti_2$ alloy.

A similar estimation of the flow stresses corresponding to Nabarro-Herring creep and power-law creep can also be made with the aid of the following equations (Ref 39, 40):

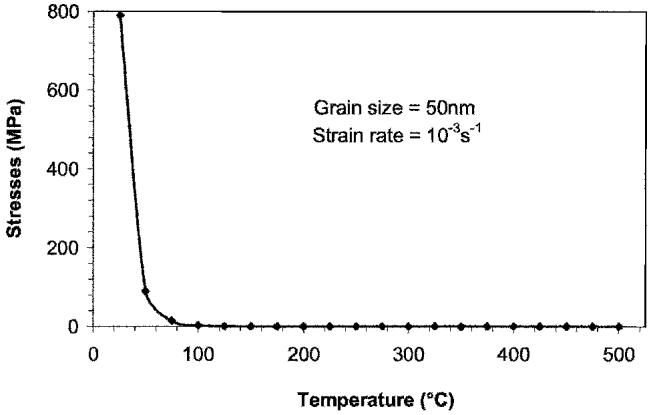

Fig. 6 Flow stress predicted using the Coble creep equation and grain boundary diffusion data of pure Al. Note that the predicted flow stresses at elevated temperatures are much lower than the experimental measurements.

$$\sigma = \dot{\varepsilon}_{Al}\frac{kT}{14\Omega}\frac{d^2}{D_v} \quad \text{(Eq 3)}$$

$$\tau = \left(\frac{\dot{\gamma}_{Al}kT}{AD_v\mu b}\right)^{1/n}\mu \quad \text{(Eq 4)}$$

where τ is the shear stress, $\dot{\gamma}_{Al}$ is the shear strain rate of the fcc-Al matrix, D_v is the lattice diffusion coefficient, μ is the shear modulus of the fcc-Al grains, b is the Burgers vector, and A is the power-law creep constant. The other parameters in Eq 3 and 4 were defined in Eq 1. The estimations using Eq 3 and 4 also result in an unambiguous conclusion that the measured flow stresses are much higher than the predicted counterparts. For instance, the predicted flow stress for Nabarro-Herring creep under an imposed strain rate of 10^{-3} s^{-1} is 0.09 MPa and for power-law creep is 13 MPa at 400 °C; in sharp contrast, the 0.2% offset yield strength measured under a strain rate of 10^{-3} s^{-1} at 400 °C is 168 MPa. Therefore, creep through lattice diffusion and dislocation climb is also suppressed in the nc $Al_{93}Fe_3Cr_2Ti_2$ alloy. The fundamental mechanisms responsible for the suppression of diffusional creep and creep dominated by dislocation climb are currently under investigation and will be discussed in the future publication.

Figure 7 shows the Young's modulus of the extruded nc $Al_{93}Fe_3Cr_2Ti_2$ alloy as a function of temperature ranging from ambient to 550 °C. For comparison, the elastic modulus of the 7075 Al alloy is also measured. It is clear that the extruded nc $Al_{93}Fe_3Cr_2Ti_2$ alloy has much higher Young's moduli than the 7075 alloy at both room and elevated temperatures. Furthermore, the elastic modulus of the 7075 alloy is very close to that of pure Al (Ref 38). The high modulus exhibited by the extruded $Al_{93}Fe_3Cr_2Ti_2$ alloy is believed to be due to the presence of 30 vol.% intermetallics. If the elastic modulus of the nc fcc-Al matrix is assumed to be equal to that of the pure Al, the average elastic modulus of the intermetallics, Al_3Ti and $Al_{13}Fe_4$, can then be estimated with the aid of the rule of mixtures:

$$E_c = 0.7E_{Al} + 0.3E_{int} \quad \text{(Eq 5)}$$

where E_c is the measured elastic modulus of the extruded $Al_{93}Fe_3Cr_2Ti_2$ alloy, E_{Al} is the elastic modulus of the nc fcc-Al matrix, and E_{int} is the average elastic modulus of the intermetallics. Using Eq 5, the average moduli of Al_3Ti and $Al_{13}Fe_4$ are estimated to be 175, 159, 147, and 140 GPa for 25, 200, 300, and 400 °C, respectively. The estimated average modulus of Al_3Ti and $Al_{13}Fe_4$ at room temperature is close to the elastic modulus of Al_3Ti predicted from the first-principle calculation (Ref 41). This lends the credence to the argument that the high elastic modulus of the nc $Al_{93}Fe_3Cr_2Ti_2$ alloy is due to the presence of the intermetallic precipitates. Nanocrystalline Al alloys with high elastic moduli and strengths can offer higher performance than traditional Al alloys in many stiffness-, strength-, and weight-critical applications (Ref 42).

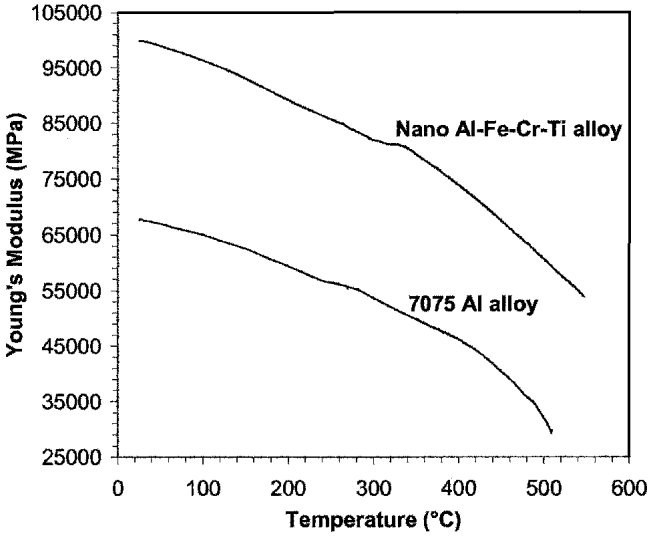

Fig. 7 Young's moduli of the extruded nc $Al_{93}Fe_3Cr_2Ti_2$ and the 7075 Al alloy as a function of temperature determined using a dynamic mechanical analyzer

4. Conclusions

The compressive strength and Young's modulus of the extruded multiphase nanocrystalline $Al_{93}Fe_3Cr_2Ti_2$ alloy were investigated. The nc $Al_{93}Fe_3Cr_2Ti_2$ alloy exhibits promising mechanical properties (i.e., superior compressive strength, ductility, and Young's modulus) at both ambient and elevated temperatures. The strength of the multiphase nc $Al_{93}Fe_3Cr_2Ti_2$ alloy increases with the decrease in the grain size at both ambient and elevated temperatures, suggesting that diffusional creep is suppressed in this alloy, even though the grain size of the alloy is below 100 nm. The dislocation-climb-dominated creep is also suppressed in this multiphase nc alloy. The superior elevated-temperature strength is believed to be due to the suppression of these creep mechanisms. The elastic modulus of the multiphase nc $Al_{93}Fe_3Cr_2Ti_2$ alloy is very high due to the presence of 30 vol.% intermetallics.

References

1. A. Inoue and H. Kimura, Fabrications and Mechanical Properties of Bulk Amorphous, Nanocrystalline, Nanoquasicrystalline Alloys in Aluminum-Based System, *J. Light Met.,* Vol 1, 2001, p 31-41
2. R.K. Islamgaliev, R.Z. Valiev, R.S. Mishra, and A.K. Mukherjee, Enhanced Superplastic Properties in Bulk Metastable Nanostructured Alloys, *Mater. Sci. Eng. A,* Vol 304-306, 2001, p 206-210
3. J. Eckert, U. Kuhn, N. Mattern, A. Reger-Leonhard, and M. Heilmaier,

Bulk Nanostructured Zr-Based Multiphase Alloys With High Strength and Good Ductility, *Scr. Mater.,* Vol 44, 2001, p 1587-1590
4. T. Mukai, S. Suresh, K. Kita, H. Sasaki, N. Kobayashi, K. Higashi, and A. Inoue, Nanostructured Al-Fe Alloys Produced by E-Beam Deposition: Static and Dynamic Tensile Properties, *Acta Mater.,* Vol 51, 2003, p 4197-4208
5. W.H. Guo and H.W. Kui, Bulk Nanostructured Alloy Formation With Controllable Grain Size, *Acta Mater.,* Vol 48, 2000, p 2117-2121
6. R.Z. Valiev, R.K. Islamgaliev, and I.V. Alexandrov, Bulk Nanostructured Materials From Severe Plastic Deformation, *Prog. Mater. Sci.,* Vol 45, 2000, p 103-189
7. H. Gleiter, Nanostructured Materials: Basic Concepts and Microstructure, *Acta Mater.,* Vol 48, 2000, p 1-29
8. Y. Wang, M. Chen, F. Zhou, and E. Ma, High Tensile Ductility in A Nanostructured Metal, *Nature,* Vol 419, 2002, p 912-915
9. J.Y. Huang, Y.K. Wu, and H.Q. Ye, Deformation Structures in Ball Milled Copper, *Acta Mater.,* Vol 44, 1996, p 1211-1221
10. G.P. Grabovetskaya, K.V. Ivanov, and Y.R. Kolobov, Creep Features of Nanostructured Materials Produced by Severe Plastic Deformation, *Ann. Chim., Sci. Mater.,* Vol 27, 2002, p 89-98
11. H. Hahn, P. Mondal, and K.A. Padmanabhan, Plastic Deformation of Nanocrystalline Materials, *Nanostructured Mater.,* Vol 9, 1997, p 603-606
12. S. Hwang, C. Nishimura, and P.G. McCormick, Deformation Mechanism of Nanocrystalline Magnesium in Compression, *Scr. Mater.,* Vol 44, 2001, p 1507-1511
13. R.K. Islamgaliev, N.F. Yunusova, I.N. Sabirov, A.V. Sergueeva, and R.Z. Valiev, Deformation Behavior of Nanostructured Aluminum Alloy Processed by Severe Plastic Deformation, *Mater. Sci. Eng. A,* Vol 319-321, 2001, p 877-881
14. Y. Ivanisenko, R.K. Wunderlich, R.Z. Valiev, and H.J. Fecht, Annealing Behaviour of Nanostructured Carbon Steel Produced by Severe Plastic Deformation, *Scr. Mater.,* Vol 49, 2003, p 947-952
15. M. Jain and T. Christman, Synthesis, Processing, and Deformation of Bulk Nanophase Fe-28Al-2Cr Intermetallic, *Acta Metall. Mater.,* Vol 42, 1994, p 1901-1911
16. H.V. Swygenhoven, M. Spaczer, D. Farkas, and A. Caro, The Role of Grain Size and the Presence of Low and High Angle Grain Boundaries in the Deformation Mechanism of Nanophase Ni: A Molecular Dynamics Computer Simulation, *Nanostructured Mater.,* Vol 12, 1999, p 323-326
17. K. Hono and T. Sakurai, Atom Probe Studies of Nanostructured Alloys, *Appl. Surf. Sci.,* Vol 87-88, 1995, p 166-178
18. A. Inoue, Fabrication and Novel Properties of Nanostructured Al Base Alloys, *Mater. Sci. Eng. A,* Vol 179-180, 1994, p 57-61
19. T.B. Massalski, *Binary Alloy Phase Diagrams,* 2nd ed. ASM International, 1990, p 147-149, 138-140, and 225-227
20. H. Mehrer, *Diffusion in Solid Metals and Alloys,* Landolt-Bornstein, New Series, Group 3, Vol 26, Springer, Berlin/Heidelbery, Germany, 1992
21. A. Inoue and H. Kimura, High-Strength Aluminum Alloys Containing Nanoquasicrystalline Particles, *Mater. Sci. Eng. A,* Vol 286, 2000, p 1-10
22. H.M. Kimura, K. Sasamori, and A. Inoue, Formation, Microstructure and Mechanical Properties of Al-Fe Base Quasicrystalline Alloys, *Mater. Sci. Eng. A,* Vol 294-296, 2000, p 168-172
23. M. Zawrah and L. Shaw, Microstructure and Hardness of Nanostructured Al-Fe-Cr-Ti Alloys Through Mechanical Alloying, *Mater. Sci. Eng. A,* Vol 355, 2003, p 37-49
24. L. Shaw, H. Luo, J. Villegas, and D. Miracle, Compressive Behavior of an Extruded Nanocrystalline Al-Fe-Cr-Ti Alloy, *Scr. Mater.,* Vol 50, 2004, p 921-925
25. P.G. Sanders, C.J. Youngdahl, and J.R. Weertman, The Strength of Nanocrystalline Metals With and Without Flaws, *Mater. Sci. Eng. A,* Vol 234-236, 1997, p 77-82
26. D. Jia, K.T. Ramesh, and E. Ma, Failure Mode and Dynamic Behavior of Nanophase Iron Under Compression, *Scr. Mater.,* Vol 42, 2000, p 73-78
27. C.C. Koch, D.G. Morris, K. Lu, and A. Inoue, Ductility of Nanostructured Materials, *MRS Bull.,* Vol 24 (No. 2), 1999, p 54-58
28. Z.-G. Yang and L. Shaw, Synthesis of Nanocrystalline SiC at Ambient Temperature Through High Energy Reaction Milling, *Nanostruct. Mater.,* Vol 7 (No. 8), 1996, p 873-886
29. L. Shaw, M. Zawrah, J. Villegas, H. Luo, and D. Miracle, Effects of Process-Control Agents on Mechanical Alloying of Nanostructured Aluminum Alloys, *Metall. Mater. Trans. A,* Vol 34A, 2003, p 159-170
30. A.L. Ortiz and L. Shaw, X-ray Diffraction Analysis of a Severely Plastically Deformed Aluminum Alloy, *Acta Mater.,* Vol 52, 2004, p 2185-2197
31. L. Shaw, H. Luo, J. Villegas, and D. Miracle, Thermal Stability of Nanostructured $Al_{93}Fe_3Cr_2Ti_2$ Alloys Prepared via Mechanical Alloying, *Acta Mater.,* Vol 51, 2003, p 2647-2663
32. R.W. Hayes, R. Rodriguez, and E.J. Lavernia, The Mechanical Behavior of a Cryomilled Al-10Ti-2Cu Alloy, *Acta Mater.,* Vol 49, 2001, p 4055-4068
33. D.L. Yaney and W.D. Nix, Elevated Temperature Deformation Behavior of an Al-8.4 Wt Pct Fe-3.6 Wt Pct Ce Alloy, *Metall. Mater. Trans. A,* Vol 18, 1987, p 893-902
34. F. Carreno and O.A. Ruano, Separated Contribution of Particles and Matrix on the Creep Behavior of Dispersion Strengthened Materials, *Acta Mater.,* Vol 46, 1998, p 159-167
35. J. Rosler, R. Joos, and E. Arzt, Microstructure and Creep Properties of Dispersion-Strengthened Aluminum Alloys, *Metall. Mater. Trans. A,* Vol 23, 1992, p 1521-1539
36. D.L. Erich, "Development of A Mechanically Alloyed Aluminum Alloy for 450-6500F Service," AFML-TR-79-4210, Air Force Research Laboratory, Dayton, OH, 1980
37. R.L. Coble, A Model for Boundary-Diffusion Controlled Creep in Polycrystalline Materials, *J. Appl. Phys.,* Vol 34, 1963, p 1679-1682
38. H.J. Frost and M.F. Ashby, *Deformation-Mechanism Maps,* Pergamon Press, Oxford, U.K., 1982
39. C. Herring, Diffusion Viscosity of a Polycrystalline Solid, *J. Appl. Phys.,* Vol 21, 1950, p 437-445
40. A.K. Mukherjee, J.E. Bird, and J.E. Dorn, Experimental Correlations for High-Temperature Creep, *Trans. ASM,* Vol 62, 1969, p 155-179
41. M.H. Yoo, C.L. Fu, and J.K. Lee, The Role of Twinning in Brittle Fracture of Ti-Alumindes, *Mat. Res. Soc. Symp. Proc.,* Vol 213, 1991, p 545-554
42. P.D. Pitcher, A.J. Shakesheff, and J.D. Lord, Aluminum Based Metal Matrix Composites for Improved Elevated Temperature Performance, *Mater. Sci. Technol.,* Vol 14, 1998, p 1015-1023